ORIGINAL ARTICLE

DOI: 10.4274/eamr.galenos.2021.94809
Eur Arch Med Res 2021;37(4):261-7

“Reversed Halo” Sign on Chest Computed Tomography in COVID-19 Pneumonia

Defne Gürbüz[1], Melis Koşar Tunç[1], Hülya Yıldız[1], Asım Kalkan[2], M. Taner Yıldırmak[3], Hakan Önder[1]

[1]University of Health Sciences Turkey, Prof. Dr. Cemil Taşcıoğlu City Hospital, Clinic of Radiology, İstanbul, Turkey
[2]University of Health Sciences Turkey, Prof. Dr. Cemil Taşcıoğlu City Hospital, Clinic of Emergency Medicine, İstanbul, Turkey
[3]University of Health Sciences Turkey, Prof. Dr. Cemil Taşcıoğlu City Hospital, Clinic of Infectious Diseases and Clinical Microbiology, İstanbul, Turkey

Abstract

Objective: The reversed halo sign (RHS) is a rare finding of chest computed tomography (CT) for coronavirus disease-2019 (COVID-19) pneumonia. This study aimed to examine the frequency and characteristics of RHS in chest CT examinations of patients with reverse transcription-polymerase chain reaction (RT-PCR)-confirmed COVID-19, to evaluate the relationship between this finding and the clinical course, and to contribute to the differential diagnosis.

Methods: Chest CT data of 1500 patients who had positive RT-PCR tests for suspected COVID-19 pneumonia between March 16, 2020, and April 26, 2020, were evaluated retrospectively. This study included 49 patients with RHS. Patients were classified into two groups as the home-treated group and hospitalized group. The number of RHS; their craniocaudal, lobar, and peripheral-central distribution; morphological features of the wall structure; change over time; and additional findings were evaluated.

Results: Of the patients with RHS, 27 (55%) were treated at home, while 22 (45%) were treated in the hospital. The number of RHS lesions was higher in the hospitalized group. Lower zone involvement and predominance were common in both groups. The home-treated group mostly had oval-shaped lesions (44%), while oval- and round-shaped lesions were common in the hospitalized group (55%). The wall thickness of the reversed halo ring was greater in the hospitalized group. Incomplete ring morphology was common in both groups. Laboratory examinations showed a significant difference between the groups in terms of the monocyte counts and C-reactive protein and D-dimer levels (p=0.04, p=0.002, and p=0.023, respectively).

Conclusion: RHS plays an important role in the differential diagnosis of COVID-19 pneumonia from other diseases based on its characteristic distribution pattern and morphological features.

Keywords: Reversed halo sign, COVID-19 pneumonia, computed tomography

INTRODUCTION

The coronavirus, which emerged in the city of Wuhan in China, has caused a respiratory tract disease called coronavirus disease-2019 (COVID-19), and it gained a pandemic status from the World Health Organization on March 11, 2020 (1). Although it most frequently presents with signs of lower respiratory tract infections such as fever, cough, and shortness of breath, clinical findings vary widely depending on the age of the patients and comorbid factors (2). Chest computed tomography (CT) plays an important role in both the diagnosis and follow-up in cases with suspected COVID-19 pneumonia (3).

In the literature, the typical involvement pattern of the lung parenchyma has been described as bilateral, multifocal, peripherally located, predominantly in the lower zone, irregularly shaped ground-glass opacities, or crazy-paving pattern characterized by interlobular septal thickening accompanied by ground-glass pattern and ground-glass opacities accompanied by consolidations. Cavitating lesions, halo sign, pleural, and

Address for Correspondence: Defne Gürbüz, University of Health Sciences Turkey, Prof. Dr. Cemil Taşcıoğlu City Hospital, Clinic of Radiology, İstanbul, Turkey
Phone: +90 533 256 07 77 **E-mail:** defnegurbuz@yahoo.com **ORCID ID:** orcid.org/0000-0003-0280-1197

Received: 15.06.2021
Accepted: 22.08.2021

Cite this article as: Gürbüz D, Koşar Tunç M, Yıldız H, Kalkan A, Yıldırmak MT, Önder H. “Reversed Halo” Sign on Chest Computed Tomography in COVID-19 Pneumonia. Eur Arch Med Res 2021;37(4):261-7

pericardial effusion, pleural thickening, and lymphadenopathy are among the findings less frequently reported (4,5).

The reversed halo sign (RHS), also known as the atoll sign and the fairy ring sign, is a chest CT finding characterized by focal ground-glass opacity surrounded by a complete or incomplete ring of consolidation in the lung parenchyma. Although rare, this finding has been previously reported in the chest CT of COVID-19 pneumonia cases (6,7).

This study aimed to contribute to the diagnosis of COVID-19 and shed light on the differential diagnosis by examining the chest CT scans of patients with reverse-transcription-polymerase chain reaction (RT-PCR)-confirmed COVID-19 and to evaluate the frequency and characteristics of the RHS in these cases, the disease stage at which the sign is observed, and the clinical course of the patients with this sign.

METHODS

The study was approved by the Ethics Review Board of University of Health Sciences Turkey, Prof. Dr. Cemil Tascioglu City Hospital (approval no: 48670771-514.10), and written informed consent was obtained from all participants who were briefed about the study. The study was conducted in accordance with the principles of the Declaration of Helsinki.

Patient Selection

Chest CT scans of 1,500 patients with positive RT-PCR tests performed for suspected COVID-19 pneumonia between March 16, 2020, and April 26, 2020, were retrospectively evaluated. Forty-nine patients with RHSs on chest CT were included in the study. Laboratory results such as C-reactive protein (CRP), D-dimer, lactate dehydrogenase, oxygen saturation (SpO_2), and lymphocyte, monocyte, and neutrophil counts of the patients were also evaluated. Patients were divided into two groups according to the treatment and follow-up protocols, namely, home-treated and hospitalized groups (service-intensive care unit follow-up).

CT Protocol and Imaging Evaluation

Chest CT scans were obtained using a Philips Ingenuity 128 Slice CT machine (Philips, Amsterdam, Netherlands), without the use of an intravenous contrast agent. Scans were completed in the supine position in a single breath-holding period with both lungs covering the area from the apices of the lungs to the costodiaphragmatic sinuses. Chest CT acquisition parameters included tube voltage of 120 kV, tube current of 200 mAs, pitch of 1.375, field of view of 512 mm, and section thickness of 1.25 mm. The number of RHSs and their localization according to the lung lobes and central/peripheral localization, morphological findings such as regularity/irregularity of the wall structure and wall thickness, complete/incomplete ring structure, nodular/reticular structure, their change over time, other patterns of COVID-19 pneumonia, and additional findings such as lymphadenopathy and pleural effusion were evaluated in the study. Images were evaluated separately by two radiologists experienced in thoracic radiology, and a decision was made with consensus.

Statistical Analysis

Statistical analyses were performed using SPSS version 22.0 statistical software IBM SPSS Statistics for Windows, version XX (IBM Corp., Armonk, N.Y., USA). The relationship between categorical data was evaluated using the chi-square test. The compliance of the data to normal distribution was determined by the Kolmogorov-Smirnov test. Student's t-test was used for the comparison of the means of two independent groups that follow a normal distribution, while the Mann-Whitney U test was used for data that deviated from the normal distribution. For the evaluation of relationships between continuous data, the Pearson's correlation test was used for data with normal distribution, while the Spearman correlation test was used for data that deviated from the normal distribution. The results are assumed to be statistically significant when p value is less than 0.05.

RESULTS

A total of 49 patients [20 (41%) were female and 29 (59%) were male] were included in this study. Of these patients, 27 (55%) were treated at home, while 22 (45%) were hospitalized. The mean age of all patients was 46.06±14.1 years. The mean age of the hospitalized group was 55.6±14.2 years, while that of the home-treated group was 38.8±9 years. The mean hospitalization period was 13.9±12.7 days [range: (2, 58) days]. Regarding additional diseases in both groups, 26 (53%) patients had no additional disease, four (8%) had hypertension, and three (6%) had both diabetes and hypertension. The remaining patients had other diseases such as hypothyroidism, epilepsy, chronic renal failure, asthma, and cardiovascular disease.

Table 1 shows the symptoms, SpO_2, lactate dehydrogenase level, CRP level, and neutrophil, lymphocyte, and monocyte counts upon admission. Cough was the most common symptom in the home-treated and hospitalized groups (70% and 60%, respectively). Regarding symptoms, a significant difference was found only in the presence of dyspnea ($p=0.02$), with unsurprisingly higher frequency in the hospitalized group. Symptoms such as sore throat, loss of appetite, abdominal pain, and diarrhea were not detected at the first admission in any of the patients in the home-treated group. In addition, cough and fatigue symptoms at the first admission were more common in the home-treated group, but the difference was not significant ($p>0.05$). SpO_2 was lower in the hospitalized group than in the home-treated group, but the difference was not significant ($p>0.05$). The difference between the laboratory test results of the groups in terms of the CRP level, D-dimer level, and monocyte count was significant ($p=0.002$, $p=0.023$, and $p=0.04$, respectively).

The localization and morphological characteristics of the RHS are given in Table 2. The frequency of the RHSs was higher in the hospitalized group than in the home-treated group [95% confidence interval (CI) 3.77-9.63; 3.16-5.64, respectively]. In regards to craniocaudal distribution, involvement of the lower zone was more common than involvement of the other zones in both groups. In addition, no significant difference was found between the two groups in terms of the craniocaudal distribution ($p>0.05$). The bilateral incidence rate of the disease was high in both groups. Regarding the lobar distribution of the disease, involvement of the lower lobes of the right and left lungs (82% and 78%, respectively) was more frequent in all patients. In the morphological examination of the reversed halo lesion, the lesion was most frequently oval-shaped in the home-treated group (44%), while lesions were oval and round in the hospitalized group (55%). Considering the ring structure of the RHS, the wall thickness was greater in the hospitalized group; however, the difference was not significant ($p>0.05$). Incomplete ring morphology of the lesion was common in both groups.

The 95% CIs for all variables of interest are presented in Table 1 and 2. An appreciable overlap was found in the CIs (e.g., cough, fatigue, and SpO_2) of the corresponding variables in both groups when the results are not significant (i.e., $p>0.05$). These intervals are mostly disjoint (e.g., dyspnea, CRP, D-dimer, and number of reversed halo lesions) when the results are significant (i.e., $p\leq0.05$).

DISCUSSION

The RHS is a rare finding in various diseases and at different disease stages. In our study, the lesions characterized with the RHS in COVID-19 pneumonia were mostly peripheral, localized in the lower lobe, irregularly contoured, oval-shaped, had a central

Table 1. Distribution of symptoms and laboratory markers in both groups of patients with reversed halo signs

	Home-treated patients (n=27)		**Hospital-treated patients (n=22)**		**All patients (n=49)**	
Symptoms	**Number (proportion)**	**95% CI**	**Number (proportion)**	**95% CI**	**Number (proportion)**	**95% CI**
Cough	19 (0.70)	0.53-0.88	13 (0.59)	0.39-0.80	32 (0.65)	0.52-0.79
Fatigue	10 (0.37)	0.19-0.55	7 (0.32)	0.12-0.51	17 (0.35)	0.21-0.48
Fever	6 (0.22)	0.07-0.38	6 (0.27)	0.09-0.46	12 (0.24)	0.12-0.37
Sore throat	0 (0.0)	0.00-0.00	2 (0.09)	-0.03-0.21	2 (0.04)	-0.01-0.10
Dyspnea	3 (0.11)	-0.01-0.23	7 (0.32)	0.12	10 (0.20)	0.09-0.32
Nausea/vomiting	2 (0.07)	-0.02-0.17	2 (0.09)	-0.03-0.21	4 (0.08)	0.00-0.16
Loss of appetite	0 (0.0)	0.00-0.00	2 (0.09)	-0.03-0.21	2 (0.04)	-0.01-0.10
Back pain	1 (0.04)	-0.03-0.11	2 (0.09)	-0.03-0.21	3 (0.06)	-0.01-0.13
Abdominal pain	0 (0.0)	0.00-0.00	1 (0.05)	-0.04-0.13	1 (0.02)	-0.02-0.06
Diarrhea	0 (0.0)	0.00-0.00	1 (0.05)	-0.04-0.13	1 (0.02)	-0.02-0.06
Asymptomatic	2 (0.07)	-0.02-0.17	1 (0.05)	-0.04-0.13	3 (0.06)	-0.01-0.13
Laboratory findings	**Mean (SD)**	**95% CI**	**Mean (SD)**	**95% CI**	**Mean (SD)**	**95% CI**
SpO_2 (%)	96.1 (3.1)	94.93-97.27	90.36 (16.9)	83.3-97.42	93.5 (11.6)	90.25-96.75
CRP	6.6 (6.5)	4.15-9.05	94.9 (79)	61.89-127.91	75.3 (78.8)	53.24-97.36
D-dimer	155.5 (6.3)	153.12-157.88	1380.3 (1623.7)	701.8-2058.8	1263.7 (1583.8)	820.24-1707.16
LDH	214.3 (28)	203.74-224.86	245.1 (53.9)	222.58-267.62	241.2 (52)	226.64-255.76
Neutrophil 10^3/µL*	5.5 (2.9)	4.41-6.59	4.8 (2.2)	3.88-5.72	5.2 (2.6)	4.47-5.93
Lymphocyte 10^3/µL*	1.6 (1.3)	1.11-2.09	2.7 (4.2)	0.94-4.46	2.1 (2.9)	1.29-2.91
Monocyte 10^3/µL*	0.3 (0.1)	0.26-0.34	0.5 (0.2)	0.42-0.58	0.4 (0.2)	0.34-0.46

*Reference values: Neutrophil: 2-7, lymphocyte: 0.8-4, monocyte: 0.12-1.2, 95% CI are for the symptom proportions and laboratory marker values, **Difference statistically significant ($p<0.05$), SpO_2 (%): Oxygen saturation, SD: Standard deviation, CI: Confidence interval, CRP: C-reactive protein, LDH: Lactate dehydrogenase reticular pattern, and had an incomplete ring presentation (Figure 1). Although the RHS is considered specific for organized pneumonia, it was detected in approximately 19% of cryptogenic organized pneumonia cases (Figure 2) (8). In the differential diagnosis of diseases with this finding, a pleural-based RHS is predominantly located in the lower lobe (especially in the costodiaphragmatic angle); the triangular-pyramidal wedge-shaped configuration suggests pulmonary embolism (Figure 3) (9); the presence of a nodular pattern in the wall and central part suggests granulomatous diseases such as tuberculosis and sarcoidosis (Figure 4) (10); predominant upper lobe involvement, thick ring structure, and presence of accompanying pleural effusion suggest fungal infections (11).

This study analyzed two groups of patients with COVID-19 divided according to the follow-up protocol (home vs. hospital). A significant difference was found in the lung parenchymal infiltration between the two groups; however, no significant difference was found in the reversed halo lesion load. In both groups, the lesion pattern in the lung parenchyma, excluding the RHS, was most frequently consolidations accompanying ground-glass opacities, which is in line with the literature. The frequency of consolidations tends to increase, especially in patients followed in the hospital and those with severe clinical and laboratory findings. This may suggest that the situation may result from the progression of ground-glass opacities to consolidations.

Table 2. Morphological features, localization, and distribution of the lesion in both groups of patients with reversed halo signs

	Home-treated patients (n=27)		**Hospital-treated patients (n=22)**		**All patients (n=49)**	
	Number (proportion)	**95% CI**	**Number (proportion)**	**95% CI**	**Number (proportion)**	**95% CI**
Craniocaudal distribution						
Upper zone	3 (0.11)	-0.01-0.23	4 (0.18)	0.02-0.34	7 (0.14)	0.04-0.24
Middle zone	7 (0.26)	0.09-0.42	3 (0.14)	-0.01-0.28	10 (0.20)	0.09-0.32
Lower zone	13 (0.48)	0.29-0.67	9 (0.41)	0.20-0.61	22 (0.45)	0.31-0.59
Diffuse involvement	4 (0.15)	0.01-0.28	6 (0.27)	0.09-0.46	10 (0.20)	0.09-0.32
Laterality						
Unilateral	3 (0.11)	-0.01-0.23	2 (0.09)	-0.03-0.21	5 (0.10)	0.02-0.19
Bilateral	24 (0.89)	0.77-1.01	20 (0.91)	0.79-1.03	44 (0.90)	0.81-0.98
Lobar distribution						
RUL	14 (0.52)	0.33-0.71	14 (0.64)	0.44-0.84	28 (0.57)	0.43-0.71
RML	3 (0.11)	-0.01-0.23	7 (0.32)	0.12-0.51	10 (0.20)	0.09-0.32
RLL	21 (0.78)	0.62-0.93	19 (0.86)	0.72-1.01	40 (0.82)	0.71-0.92
LUL	8 (0.30)	0.12-0.47	10 (0.45)	0.25-0.66	18 (0.37)	0.23-0.50
LLL	19 (0.70)	0.53-0.88	19 (0.86)	0.72-1.01	38 (0.78)	0.66-0.89
Lesion morphology						
Shape						
Round	6 (0.22)	0.07-0.38	6 (0.27)	0.09-0.46	12 (0.24)	0.12-0.37
Oval	12 (0.44)	0.26-0.63	4 (0.18)	0.02-0.34	16 (0.33)	0.20-0.46
Round and oval	9 (0.33)	0.16-0.51	12 (0.55)	0.34-0.75	21 (0.43)	0.29-0.57
Ring structure						
Incomplete	16 (0.59)	0.41-0.78	9 (0.41)	0.20-0.61	25 (0.51)	0.37-0.65
Complete	6 (0.22)	0.07-0.38	4 (0.18)	0.02-0.34	10 (0.20)	0.09-0.32
Incomplete and complete	5 (0.19)	0.04-0.33	9 (0.41)	0.20-0.61	14 (0.29)	0.16-0.41
	Mean (SD)	**95% CI**	**Mean (SD)**	**95% CI**	**Mean (SD)**	**95% CI**
Number of reversed halo lesions	4.4 (3.3)	3.16-5.64	6.7 (7)	3.77-9.63	5.4 (4.4)	4.17-6.63
Lesion wall thickness	4.1 (1.6)	3.50-4.70	4.2 (2.4)	3.20-5.20	4.2 (2)	3.64-4.76

95% CI are for the symptom proportions and laboratory marker values, SD: Standard deviation, CI: Confidence interval, RUL: Right upper lobe, RML: Right middle lobe, RLL: Right lower lobe, LUL: Left upper lobe, LLL: Left lower lobe

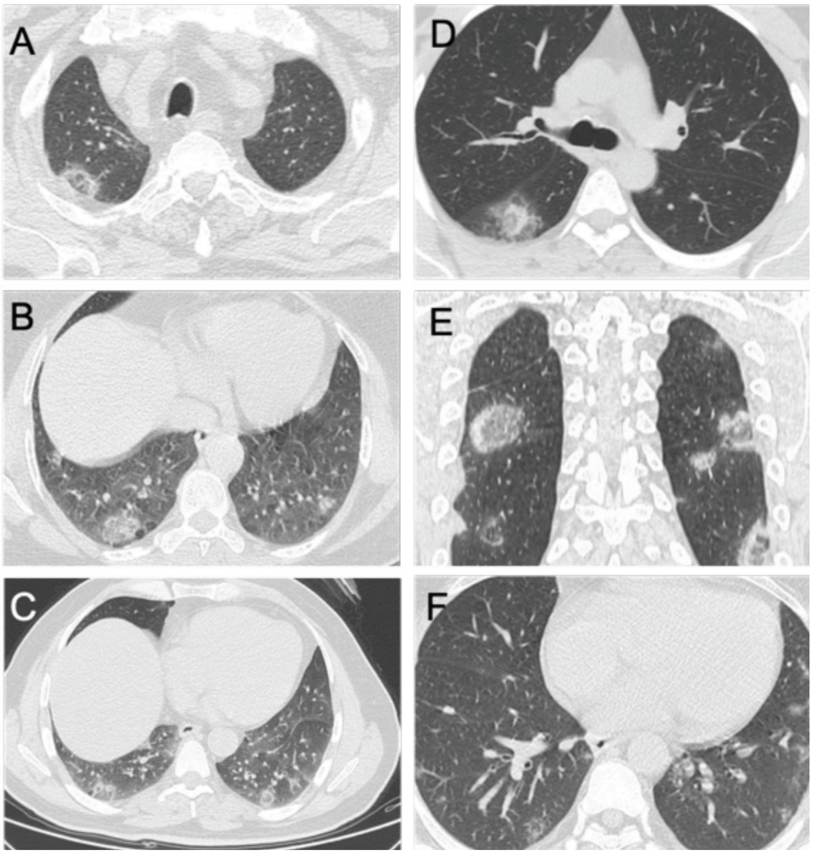

Figure 1. Cases with findings of COVID-19 pneumonia on chest CT with positive reverse-transcription-polymerase chain reaction results. Chest CT images of a 68-year-old male patient reveal peripherally located ground-glass opacity areas and multiple reversed halo signs of different sizes (A-C). Other patients demonstrated lesions characterized with the reversed halo sign in the superior segment of the right lung lower lobe (D), multiple lesions with peripheral localization in the bilateral lung parenchyma (E), and bilateral millimetric lesions with faint contours in the lower lobes (F)
CT: Computed tomography, COVID-19: Coronavirus disease-2019

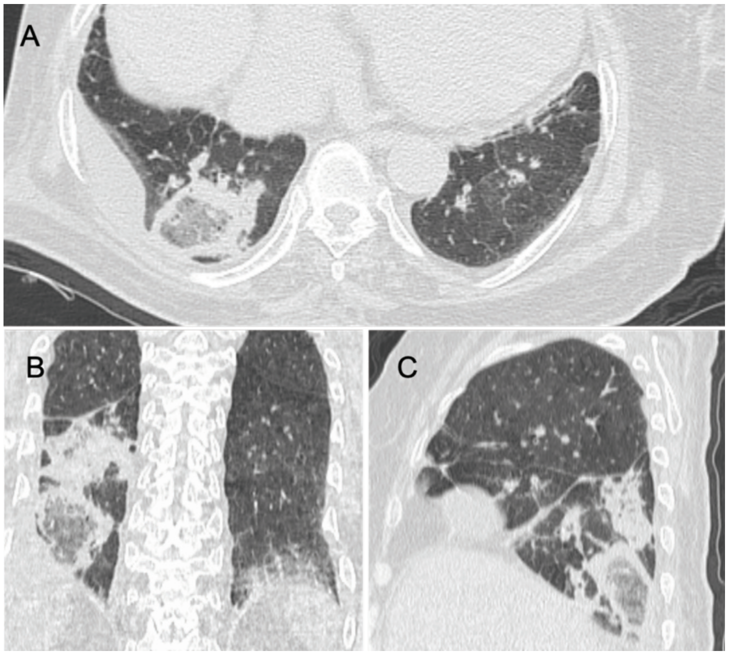

Figure 2. Axial (A) chest computed tomography in a patient with cryptogenic organized pneumonia shows a reversed halo sign in the posterior segment of the lower lobe of the right lung, with an adjacent irregularly contoured patchy area of consolidation, which is more clearly distinguished in the coronal (B) and sagittal (C) planes

According to our findings, incomplete morphology was observed in the RHS of the home-treated group; in other words, the ground-glass component was dominant over the consolidated wall. In the hospitalized group, a more heterogeneous pattern was observed with complete and incomplete morphology seen together. The wall thickness of the reversed halo lesion was significantly higher in the hospitalized group than in the home-treated group. These findings may suggest that the RHS was seen in earlier stages of COVID-19 and the lesions progressed to consolidations afterwards. Moreover, in our study, no additional disease was found in 26 (53%) patients with the RHS, mainly in the home-treated group. This may indicate the occurrence of the RHS in patients with less comorbidity.

The clinical course of COVID-19 pneumonia is quite variable; individuals may have no symptoms or have mild flu-like symptoms, and some may have an extremely poor prognosis. The inflammatory cascade triggered by COVID-19 infection, cytokine release, and activation of the coagulation cascade are

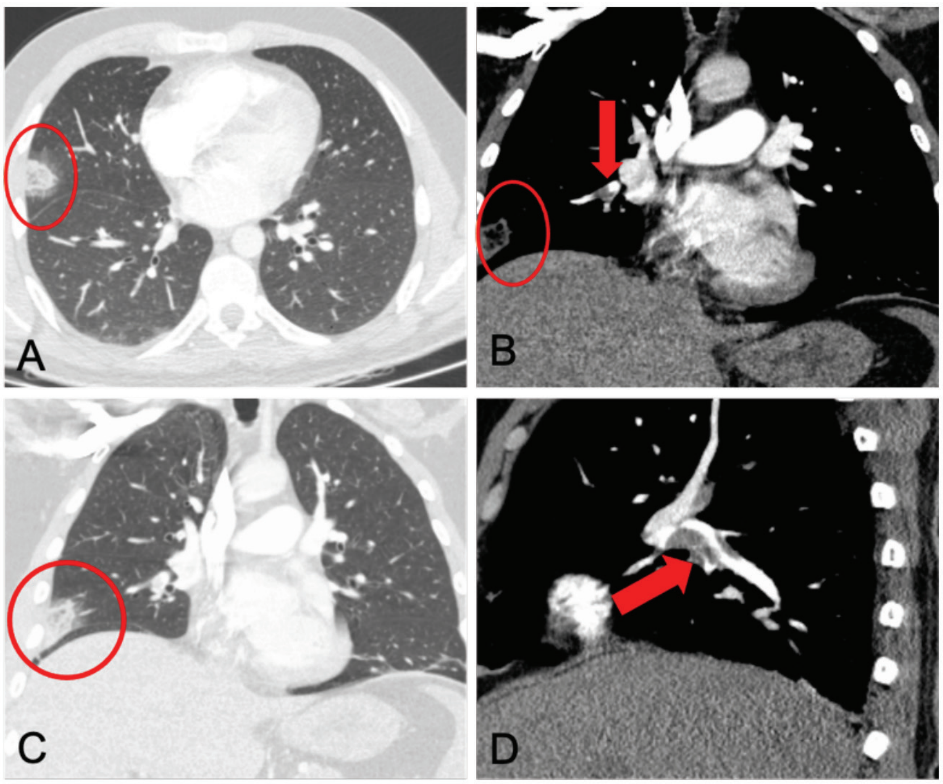

Figure 3. Axial (A) and coronal (C) chest CT sections revealed a pleural-based, triangular-shaped reversed halo sign (circled) in the lateral segment of the middle lobe of the right lung consistent with pulmonary infarction. Mediastinal window coronal (B) and sagittal (D) sections of pulmonary CT angiography show clot formation extending from the right descending interlobar artery to the middle lobe lateral segmentary branch (arrow)
CT: Computed tomography

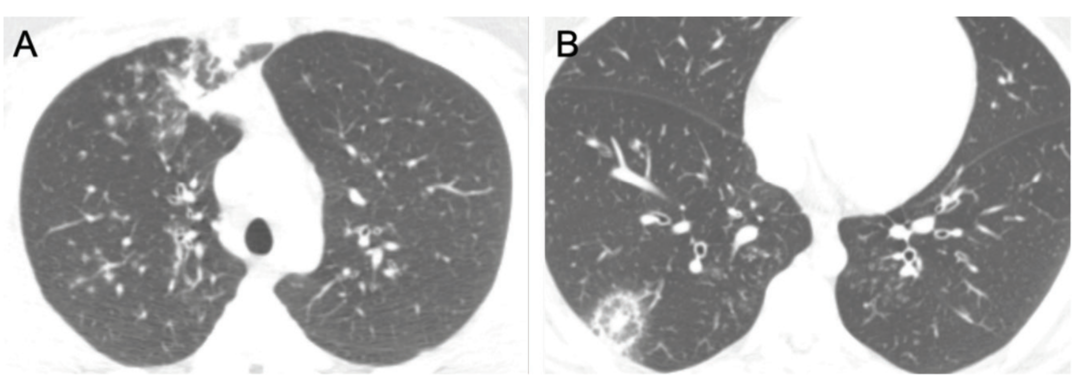

Figure 4. Axial chest computed tomography scans of a 38-year-old patient diagnosed with sarcoidosis reveal multiple millimetric nodules with faint contours, adjacent faint ground-glass opacities, and focal subpleural fibrotic changes in the right lung upper lobe (A) and reversed halo sign with nodularity on the wall and in the central region in the right lung lower lobe and millimetric centrilobular nodules on both lung lower lobes (B)

the mechanisms held responsible for a poor prognosis (12). In addition, the use of risk classifications based on comorbid factors and laboratory markers have been recommended to predict the clinical course of the disease (12-15). The levels of CRP, which indicate hyperinflammation in critically affected cases, procalcitonin, D-dimer, and ferritin are increased in some cases (16-18). In this study, a significant difference was found in the CRP level, D-dimer level, and monocyte count between the home-treated group and hospitalized group. Our findings also indicate a positive correlation between these laboratory markers and the lesion load characterized by the RHS. In this respect, the RHS detected in CT examination, which is frequently used in diagnosis, may contribute to the prediction of prognosis in these cases.

CONCLUSION

The RHS plays an important role in the differential diagnosis of COVID-19 pneumonia from other diseases based on its characteristic distribution pattern and morphological features. In addition, studies with larger patient groups are needed to evaluate whether this rare radiological finding can be used as a prognostic factor.

Ethics

Ethics Committee Approval: The study was approved by the Ethics Review Board of University of Health Sciences Turkey, Prof. Dr. Cemil Tascioglu City Hospital (approval no: 48670771-514.10).

Informed Consent: Written informed consent was obtained from all participants who were briefed about the study.

Peer-review: Externally peer-reviewed.

Authorship Contributions

Concept: D.G., M.K.T., Design: D.G., M.K.T., Data Collection or Processing: D.G., M.K.T., H.Y., A.K., M.T.Y., H.Ö., Analysis or Interpretation: D.G., M.K.T., Literature Search: D.G., M.K.T., Writing: D.G., M.K.T., H.Y., A.K., M.T.Y., H.Ö.

Conflict of Interest: No conflict of interest was declared by the authors.

Financial Disclosure: The authors declared that this study received no financial support.

REFERENCES

1. Cucinotta D, Vanelli M. WHO Declares COVID-19 a Pandemic. Acta Biomed 2020;91:157-60.
2. Harapan H, Itoh N, Yufika A, Winardi W, Keam S, Te H, et al. Coronavirus disease 2019 (COVID-19): A literature review. J Infect Public Health 2020;13:667-73.
3. Ye Z, Zhang Y, Wang Y, Huang Z, Song B. Chest CT manifestations of new coronavirus disease 2019 (COVID-19): a pictorial review. Eur Radiol 2020;30:4381-49.
4. Carotti M, Salaffi F, Sarzi-Puttini P, Agostini A, Borgheresi A, Minorati D, et al. Chest CT features of coronavirus disease 2019 (COVID-19) pneumonia: key points for radiologists. Radiol Med 2020;125:636-46.
5. Li Y, Xia L. Coronavirus disease 2019 (COVID-19): role of chest CT in diagnosis and management. AJR Am J Roentgenol 2020;214:1280-6.
6. Shaghaghi S, Daskareh M, Irannejad M, Shaghaghi M, Kamel IR. Target-shaped combined halo and reversed-halo sign, an atypical chest CT finding in COVID-19. Clin Imaging 2021;69:72-74.
7. Poerio A, Sartoni M, Lazzari G, Valli M, Morsiani M, Zompatori M. Halo, reversed halo, or both? Atypical computed tomography manifestations of coronavirus disease (COVID-19) pneumonia: the “double halo sign”. Korean J Radiol 2020;21:1161-4.
8. Kim SJ, Lee KS, Ryu YH, Yoon YC, Choe KO, Kim TS, et al. Reversed halo sign on high-resolution CT of cryptogenic organizing pneumonia: diagnostic implications. AJR Am J Roentgenol 2003;180:1251-4.
9. Casullo J, Semionov A. Reversed halo sign in acute pulmonary embolism and infarction. Acta Radiol 2013;54:505-10.
10. Godoy MC, Viswanathan C, Marchiori E, Truong MT, Benveniste MF, Rossi S, et al. The reversed halo sign: update and differential diagnosis. Br J Radiol 2012;85:1226-35.
11. Wahba H, Truong MT, Lei X, Kontoyiannis DP, Marom EM. Reversed halo sign in invasive pulmonary fungal infections. Clin Infect Dis 2008;46:1733-7.
12. Ponti G, Maccaferri M, Ruini C, Tomasi A, Ozben T. Biomarkers associated with COVID-19 disease progression. Crit Rev Clin Lab Sci 2020;57:389-9.
13. Richardson S, Hirsch JS, Narasimhan M, Crawford JM, McGinn T, Davidson KW, et al. Presenting characteristics, comorbidities, and outcomes among 5700 patients hospitalized with COVID-19 in the New York City area. JAMA 2020;323:2052-9.
14. Huang I, Lim MA, Pranata R. Diabetes mellitus is associated with increased mortality and severity of disease in COVID-19 pneumonia - a systematic review, meta-analysis, and meta-regression. Diabetes Metab Syndr 2020;14:395-403.
15. Pranata R, Huang I, Lim MA, Wahjoepramono EJ, July J. Impact of cerebrovascular and cardiovascular diseases on mortality and severity of COVID-19-systematic review, meta-analysis, and meta-regression. J Stroke Cerebrovasc Dis 2020;29:104949.
16. Huang I, Pranata R, Lim MA, Oehadian A, Alisjahbana B. C-reactive protein, procalcitonin, D-dimer, and ferritin in severe coronavirus disease-2019: a meta-analysis. Ther Adv Respir Dis 2020;14:1753466620937175.
17. Chen N, Zhou M, Dong X, Qu J, Gong F, Han Y, et al. Epidemiological and clinical characteristics of 99 cases of 2019 novel coronavirus pneumonia in Wuhan, China: a descriptive study. Lancet 2020;395:507-13.
18. Ji W, Bishnu G, Cai Z, Shen X. 2020 Mar 13. Analysis Clinical Features of COVID-19 Infection in Secondary Epidemic Area and Report Potential Biomarkers in Evaluation. medRxiv 2020.03.10.20033613.